

## ON THE FORMATION OF EXTENDED GALACTIC DISKS BY TIDALLY DISRUPTED DWARF GALAXIES

JORGE PEÑARRUBIA , ALAN MCCONNACHIE & ARIF BABUL  
 University of Victoria, 3800 Finnerty Rd., Victoria, BC, V8P 5C2, Canada  
*Draft version July 30, 2018*

### ABSTRACT

We explore the possibility that extended disks, such as that recently discovered in M31, are the result of a single dwarf ( $10^9$ – $10^{10}M_\odot$ ) satellite merger. We conduct N-body simulations of dwarf NFW halos with embedded spheroidal stellar components on co-planar, prograde orbits in a M31-like host galaxy. As the orbit decays due to dynamical friction and the system is disrupted, the stellar particles relax to form an extended, exponential disk-like structure that spans the radial range 30–200 kpc. The disk scale-length  $R_d$  correlates with the initial extent of the stellar component within the satellite halo: the more embedded the stars, the smaller the resulting disk scale-length. If the progenitors start on circular orbits, the kinematics of the stars that make up the extended disk have an average rotational motion that is 30 – 50 km/s lower than the host’s circular velocity. For dwarf galaxies moving on highly eccentric orbits ( $e \simeq 0.7$ ), the stellar debris exhibits a much lower rotational velocity. Our results imply that extended galactic disks might be a generic feature of the hierarchical formation of spiral galaxies such as M31 and the Milky Way.

*Subject headings:* stellar dynamics – methods: N-body simulations– methods: semi-analytical – galaxies: kinematics and dynamics – galaxies: halos – galaxies: dwarfs

### 1. INTRODUCTION

Within the context of the hierarchical formation scenario, galaxies such as M31 are expected to have assimilated 100–500 smaller mass systems over a Hubble time (e.g. Moore et al 1999). Today, stars from these systems are expected to be found in the disk, bulge and stellar halo (e.g Abadi et al. 2003, 2006, Governato et al. 2004 and references therein). The fossil signatures of these remnants are a veritable treasure trove of information about the galaxy assembly process and the nature of the merging subunits.

Detailed investigations of M31 (Ibata et al. 2001, 2004, 2005, Ferguson et al. 2002, 2005, McConnachie et al. 2003, 2004, Zucker et al. 2004, Fardal et al. 2006, Font et al. 2006, Guhathakurta et al. 2006, Kalirai et al. 2006, Brown et al. 2006, Chapman et al. 2006) reveal a large number of fossil substructures. Intriguingly, many of these have disk kinematics and are distributed in a gigantic flattened structure surrounding the high-surface brightness inner disk (Ibata et al. 2005). The observations are consistent with this extended structure being a rotating disk-like system whose midplane is coincident with that of the inner disk, but which extends  $\gtrsim 80$  kpc from the center of M31. The rotational velocities of the constituent stars lag the M31 disk rotation by  $\sim 30$  km/s (Ibata et al. 2005). The mass of the extended disk is  $\sim 10\%$  of the inner disk and its stellar surface density profile of the structure is consistent with an exponential decline although there is some uncertainty about the value of the radial scale length (cf. Ibata et al 2005; Kalirai et al. 2006). Here, we explore whether the extended disk could be the remnant of a dwarf galaxy.

### 2. CONSTRUCTING OUR GALAXY MODELS

#### 2.1. The host galaxy

Our M31 galaxy model consists of three static sub-components: a Miyamoto-Nagai (1975) disk, a spherical Hernquist (1990) bulge and a spherical Navarro, Frenk

& White (1997) (NFW) dark matter halo. The corresponding potentials are:

$$\Phi_d = -\frac{GM_d}{\sqrt{R^2 + (a + \sqrt{z^2 + b^2})^2}}; \quad \Phi_b = -\frac{GM_b}{r+c};$$

$$\Phi_h = -\frac{GM_h \ln(1+r/r_s)}{r} \left[ \ln(1+c_{200}) - \frac{c_{200}}{1+c_{200}} \right]^{-1} \quad (1)$$

Following Geehan et al. (2005), we set  $M_d = 8.4 \times 10^{10}M_\odot$ ,  $M_b = 3.3 \times 10^{10}M_\odot$ ,  $a = 5.4$  kpc,  $b = 0.26$  kpc and  $c = 0.61$  kpc. The M31 halo parameters are  $M_h(r_{200}) = 6.8 \times 10^{11}M_\odot$ ,  $r_{200} = 180$  kpc,  $r_s = 8.18$  kpc, which yields a concentration of  $c_{200} = r_{200}/r_s = 22$ .

#### 2.2. Generating N-body satellite galaxies in equilibrium

Our satellite models have two components: (i) a spherical NFW dark matter halo, (ii) an embedded spherical “stellar” component that reproduces a King (1966) density distribution and approximates the light profile of the dSph galaxies of the Milky Way (MW) and M31 (Irwin & Hatzidimitriou 1995, McConnachie & Irwin 2006).

We use the code of Kazantzidis et al. (2004, 2006) to generate NFW satellite halos with  $10^6$  particles,  $c = r_{\text{vir}}/r_s = 20$  and an exponential cut-off at the virial radius. We calculate the relative energy,  $\epsilon = \Psi - v^2/2$ , and the relative potential,  $\Psi = -\Phi_{\text{NFW}} + \Phi_{\text{NFW}}(\infty)$ , for all satellite particles. Next, we generate  $n$  bins in energy and, for each bin, we select  $f_*(\epsilon)/f_{\text{NFW}}(\epsilon) \times N(\epsilon)$  “stellar” particles, where  $N(\epsilon)$  is the number of NFW particles within  $(\epsilon, \epsilon + d\epsilon)$  and  $d\epsilon = \epsilon_{\text{max}}/n$ . Here,  $f_*$  and  $f_{\text{NFW}}$  are the isotropic distribution function for the stellar and the dark matter particles calculated from

$$f_i(\epsilon) = \frac{1}{8\pi^2} \left[ \int_0^\epsilon \frac{d^2\rho_i}{d\Psi^2} \frac{d\psi}{\sqrt{\epsilon - \Psi}} + \frac{1}{\sqrt{\epsilon}} \left( \frac{d\rho_i}{d\Psi} \right)_{\Psi=0} \right], \quad (2)$$

where the subscript  $i$  denotes that  $\rho$  can be either a NFW

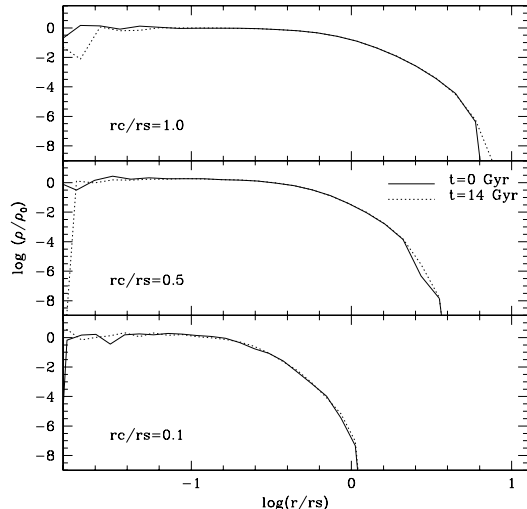


FIG. 1.— Density profile of the stellar component normalized to the central density ( $\rho_0$ ). Solid and dotted lines show respectively the profiles at  $t = 0$  and after 14 Gyr of evolution in isolation (i.e. in absence of external forces). Our method to embed a “stellar” profile within a NFW halo produces systems in equilibrium.

or a King profile. The result is  $N_\star$  dark matter particles with a density distribution

$$\rho_\star = \frac{K}{x^2} \left[ \frac{\cos^{-1}(x)}{x} - \sqrt{1-x^2} \right], \quad x \equiv \frac{1 + (r/r_c)^2}{1 + (r/r_t)^2}. \quad (3)$$

$r_c$  and  $r_t$  are the core and tidal radii,  $K$  is an arbitrary constant, and we have fixed  $r_t/r_c = 5$  (see Bullock & Johnston (2005) for more details). By construction, the stellar component does not contribute to the potential of the satellite galaxy, nor does it influence its evolution.

### 2.3. Satellite structural and orbital parameters

We consider satellites with mass  $M[r_{\text{vir}}] = 5 \times 10^9 M_\odot$  (model H1), the estimated mass of typical Local Group dwarf galaxies, and  $M[r_{\text{vir}}] = 5 \times 10^{10} M_\odot$  (model H2), at the top end of minor mergers in merger trees for a M31-like galaxy. Different King profiles are used for the tracer stellar particles, characterized by the quantity  $r_c/r_s$ . This determines the compactness of the stellar component in the halos. We select  $r_c/r_s = 1.0, 0.5, 0.1$  (K1, K2 and K3, respectively). The number of stellar particles available to trace the King profiles decreases as  $r_c/r_s$  decreases, so that  $N_\star = 3.1 \times 10^5, 1.3 \times 10^5, 1.5 \times 10^4$  for K1, K2 and K3, respectively.

Satellites are placed in the host galaxy at an initial apocenter of  $r_a = 75$  kpc. The velocity is chosen to obtain the desired orbital eccentricity. We explore (i) an initially circular orbit, and (ii) a highly eccentric orbit ( $e = [r_a - r_p]/[r_a + r_p] = 0.71$ , or  $r_a/r_p = 1/6$ , where  $r_a$  and  $r_p$  are the apo and peri center distances). The latter corresponds to the typical eccentricity of satellite galaxies in cosmological simulations (Ghigna et al. 1998). For this Letter, we only study satellites whose orbits are co-planar and prograde with the M31 disk.

## 3. N-BODY SIMULATIONS

We refer the reader to Peñarrubia et al. (2006) for a detailed description of our N-body code and the numerical parameters and techniques used in our simulations. Fig. 1 shows the density profiles of K1, K2, K3 at  $t = 0$  (solid lines) and after evolving them for 14 Gyr in isolation. This shows that (i) the method outlined in §2.2 produces N-body systems in perfect equilibrium (to within Poisson fluctuations) and (ii) the selection of the N-body code’s numerical parameters is appropriate.

## 4. RESULTS

### 4.1. Disruption of satellite galaxies

The process of disruption occurs as the satellite galaxy sinks to the central regions of the host galaxy (owing to dynamical friction) and tidal forces strip the dark and stellar particles. The sequence for model K2H2 can be seen in Fig. 2: the left column shows the surface density profile of stars (filled circles) and dark matter (open circles) at different times. The right column shows the projection of stellar (black dots) and dark matter (grey dots) particles onto the disk plane of the host galaxy. The top panel shows the satellite galaxy at a time when most of the stellar material is still bound (see the corresponding right-hand panel), so that the surface density profile is fairly peaked at the satellite location. As time passes, the stellar particles start to form tidal streams, which can be seen as bumps in  $\Sigma(R)$ . As the debris configuration relaxes (mixes in phase-space), the curve  $\Sigma(R)$  smooths and approaches an exponential-like surface density profile over the interval  $30 \leq R \leq 200$  kpc. The solid line in the left panels shows the profile of an exponential disk with  $\Sigma = \Sigma_0 \exp(-R/R_d)$  and  $R_d = 30$  kpc. Since the stellar component is initially tightly bound, then the stellar surface density distribution is considerably steeper than that of dark matter particles.

The time-scale for the extended disk to form is a combination of the decay and relaxation times ( $t_{\text{dec}}$  and  $t_{\text{rel}}$ , respectively). For massive satellites (eg. Fig. 2), the satellite sinks and disrupts within  $t_{\text{dec}} \simeq 3$  Gyr. Thus, the relaxation and decay times are only comparable in the inner regions of the host galaxy. Debris at  $R \gtrsim 120$  kpc are not relaxed even after a Hubble time.

### 4.2. Spatial distribution of debris

While the above results are for a specific case, the emergence of an extended exponential disk appears to be a generic feature of the disruption of satellites on coplanar orbits. In Fig. 3, we show the surface density profiles of the stellar and dark matter particles after 14 Gyr of evolution for various combinations of satellite masses, embedded stellar systems and orbital eccentricities. The left and right columns show satellite galaxies on circular and highly eccentric orbits, respectively. Top and bottom panels are for satellite galaxies with initial masses of  $5 \times 10^9 M_\odot$  and  $5 \times 10^{10} M_\odot$ , respectively.

In the case of a lower-mass satellite on an initially circular orbit, the surface density of stellar debris is not smooth even after 14 Gyr and does not resemble exponential. This is because the satellite has a long orbital decay time. The system has disrupted relatively recently and the debris has not yet relaxed. This is in contrast to the case of a massive satellite galaxy on a highly eccentric orbit (left-bottom panel). The dynamical friction is so

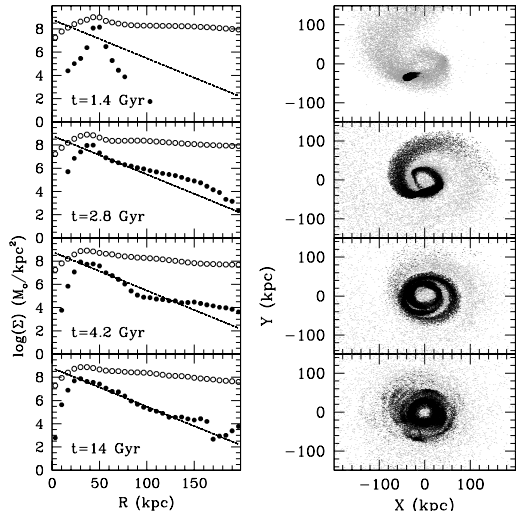


FIG. 2.— *Left column:* Surface density as a function of radius for the model K2H2 on an initially circular orbit. Stellar and dark particles are shown with filled and open circles, respectively. Each panel corresponds to a different time. The solid lines shows the surface density of an exponential disk  $\Sigma = \Sigma_0 \exp(-R/R_d)$  with  $R_d = 30$  kpc. *Right column:* Distribution of stellar (black dots) and dark matter (grey dots) debris at the same snapshots. Note how remarkably the stellar debris resemble an exponential disk after the satellite galaxy has been totally disrupted.

efficient that the satellite sinks to the galaxy center and disrupts within  $\sim 2$  Gyr. Since there is no difference in the disruption time-scales for the dark and stellar particles, both distributions are practically the same: an exponential with a large radial scale  $R_d \simeq 105$  kpc, independent of how compact the stellar system was initially.

The intermediate cases in the bottom-left (massive satellite, circular orbit) and the top-right (average-mass dwarf, eccentric orbit) panels show exponential stellar profiles over finite radius: 30 – 120 kpc for the circular orbit, and 60 – 150 kpc for the eccentric one. We find that the more compact the stellar component, the steeper the final stellar surface density profile. The scale-lengths of the exponential profiles are  $R_d \simeq 50, 30$  and 7 kpc for models with initial  $r_c/r_s = 1.0, 0.5$  and 0.1, respectively, independent of initial orbital eccentricity.

### 4.3. Debris kinematics

The extended disk in M31 was primarily identified by its rotating kinematic signature. In Fig. 4 we plot the average radial and azimuthal velocities of the satellite debris for those simulations that form an exponential-like disk after 14 Gyr (left column: massive satellite on a circular orbit; right column: typical-mass satellite on an eccentric orbit). For comparison, we also show the circular velocity curve of the host galaxy (dashed lines).

From the panels showing the mean galactocentric radial velocities, we see that the remnant of both satellites are practically relaxed, in that the stream motion in the radial direction is small. More interestingly, the extended debris exhibits a net rotation about the host galaxy center, independent of the satellite’s initial orbital eccentricity. For the satellite galaxy on an initially circular orbit, the rotational velocity of the debris is  $\sim 20 - 50$  km/s lower than the host circular velocity for  $R \gtrsim 30$  kpc.

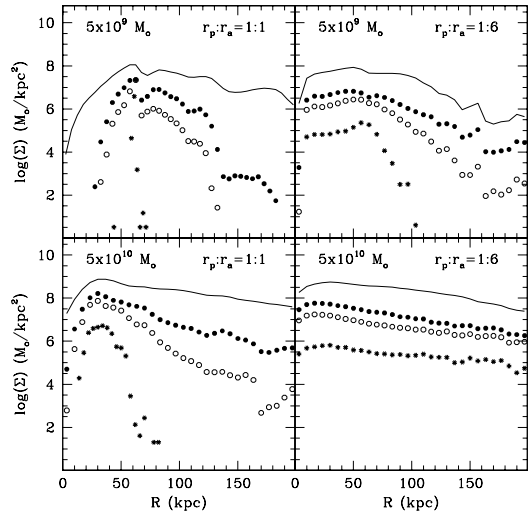


FIG. 3.— Surface density of debris as a function of radius after 14 Gyr of evolution. Models K1, K2 and K3 are represented by filled circles, open circles and stars, respectively. Left and right columns show the distribution of debris of a galaxy on a circular and a highly eccentric orbit, respectively. Strong solid lines show the distribution of dark matter particles for comparison. Note that the resulting stellar density depends on both, the dwarf orbit and its initial distribution within the halo.

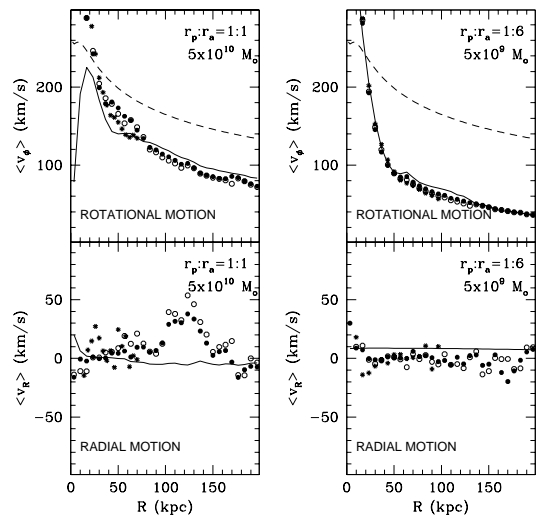


FIG. 4.— Average azimuthal (top panels) and radial (bottom panels) stellar velocities as a function of radius for models K1, K2, K3 (same notation as in Fig. 3). The left and right columns show satellites moving on a circular and a highly eccentric orbit, respectively. Note that the velocities of stellar debris are insensitive to their initial distribution within the dwarf halo but they reflect the orbital properties of the progenitor galaxy.

The satellite on an initially eccentric orbit shows a much lower rotational velocity, typically about 100 km/s lower than  $v_c$  for  $R \gtrsim 40$  kpc. Also, the stellar kinematics trace the dark matter debris, independent of the initial distribution of stars within the dwarf galaxy.

## 5. IMPLICATIONS

We find that stellar debris, resulting from the disruption of dwarf galaxies on prograde orbits which are co-

planar with the host galaxy disk, relax into an extended exponential disk. The disk scale-length is strongly correlated with the initial distribution of stars inside the dwarf halo, such that more embedded stellar profiles have smaller “disk” scale-length. For the simulations shown here,  $R_d = 50, 30$  and  $7$  kpc for the initial stellar compactness parameter  $r_c/r_s = 1.0, 0.5$  and  $0.1$ , respectively. The stellar debris exhibit rotation, even in the case of dwarf galaxies on initially highly eccentric orbits. The average rotational velocity is around  $30 - 50$  km/s lower than the host circular velocity if the satellite initially moves on a circular orbit. For highly eccentric orbits, the resulting rotational velocity is a factor  $\sim 2$  lower.

In the specific case of M31, Ibata et al. (2005) find the extended disk of M31 has a rotational velocity that is  $\sim 30$  km/s lower than  $v_c$ . Based on our results, the observed kinematics favour a scenario where the disk progenitor was a massive satellite galaxy on a low-eccentricity, low-inclination orbit, possibly similar to the progenitor of the Monoceros stream in the MW (Peñarrubia et al. 2005).

How common should such extended disks be?  $\Lambda$ CDM simulations find that spiral galaxies experience several mergers of massive,  $0.01 - 0.1 M_{\text{host}}$  dwarf galaxies (e.g. Gao et al. 2004), many on low eccentricity orbits (Ghigna et al. 1998). That extended disks appear aligned with the inner disk is not surprising taking into account the strong decrease in orbital inclination suffered by massive satellites in flattened systems (Quinn & Goodman 1986, Peñarrubia, Kroupa, Boily 2002), as well as or-

bit circularization (Jiang & Binney 2000). Thus, in a  $\Lambda$ CDM work frame, our results indicate that extended disks might be a common result of the hierarchical formation of spiral galaxies such as the MW and M31.

Would accretion destroy the inner disk? Our simulations assume a static, non-responsive host galaxy potential. Several works (Toth & Ostriker 1992, Walker, Mihos & Hernquist 1996, Velazquez & White 1999) have shown that, for sufficiently massive satellites, the inner disk would be disrupted by the merger event. To analyze this possibility we have carried out self-consistent N-body simulations of the infalling systems considered in this *Letter*. Our preliminar results indicate that the inner disk is not strongly affected by these accretion events since, owing to the nearly exponential mass-loss rate of NFW halos, the dwarf galaxies are disrupted *before* dynamical frictions brings these systems close to the inner disk. The results from these simulations, together with the analysis of the response of the inner disk, will be shown in a subsequent paper.

We thank Stelios Kazantzidis for the use of his code, and Scott Chapman, Julio Navarro, Raja Guhathakurta and Mark Fardal for useful discussions. JP thanks Julio Navarro for financial support. AB was supported by NSERC through the Discovery Grant program. AM thanks Julio Navarro and Sara Ellison for financial support.

#### REFERENCES

- Abadi, M. G., Navarro, J. F., Steinmetz, M., & Eke, V. R. 2003, *ApJ*, 597, 21
- Abadi, M. G., Navarro, J. F., & Steinmetz, M. 2006, *MNRAS*, 365, 747
- Brown, T. M., Smith, E., Guhathakurta, P., Rich, R. M., Ferguson, H. C., Renzini, A., Sweigart, A. V., & Kimble, R. A. 2006, *ApJ*, 636, L89
- Bullock J.S., Johnston K.V., 2005, *ApJ*, 635, 931
- Chapman, S. C., Ibata, R., Lewis, G. F., Ferguson, A. M. N., Irwin, M., McConnachie, A., & Tanvir, N. 2006, astro-ph/0602604 & Guhathakurta, P. 2006, *MNRAS*, 366, 1012
- Ferguson, A. M. N., Irwin, M. J., Ibata, R. A., Lewis, G. F., & Tanvir, N. R. 2002, *AJ*, 124, 1452
- Ferguson, A. M. N., Johnson, R. A., Faria, D. C., Irwin, M. J., Ibata, R. A., Johnston, K. V., Lewis, G. F., & Tanvir, N. R. 2005, *ApJ*, 622, L109
- Font, A. S., Johnston, K. V., Guhathakurta, P., Majewski, S. R., & Rich, R. M. 2006, *AJ*, 131, 1436
- Gao, L., White, S. D. M., Jenkins, A., Stoehr, F., & Springel, V. 2004, *MNRAS*, 355, 819
- Geehan J.J., Fardal M.A., Babul A., Guhathakurta P., 2005, *MNRAS*, 366, 996
- Ghigna, S., Moore, B., Governato, F., Lake, G., Quinn, T., & Stadel, J. 1998, *MNRAS*, 300, 146
- Governato, F., et al. 2004, *ApJ*, 607, 688
- Guhathakurta, P., et al. 2006, *AJ*, 131, 2497
- Hernquist L., 1990, *ApJ*, 356, 359
- Ibata, R., Irwin, M., Lewis, G., Ferguson, A. M. N., & Tanvir, N. 2001, *Nature*, 412, 49
- Ibata, R., Chapman, S., Ferguson, A. M. N., Irwin, M., Lewis, G., & McConnachie, A. 2004, *MNRAS*, 351, 117
- Ibata, R., Chapman, S., Ferguson, A. M. N., Lewis, G., Irwin, M., & Tanvir, N. 2005, *ApJ*, 634, 287
- Irwin M., Hatzidimitriou D., 1995, *MNRAS*, 277, 1354
- Jiang I., Binney J., 2000, *MNRAS*, 314, 468
- Kalirai, J. S., Guhathakurta, P., Gilbert, K. M., Reitzel, D. B., Majewski, S. R., Rich, R. M., & Cooper, M. C. 2006, *ApJ*, 641, 268
- Kazantzidis S., Magorrian J., Moore B., 2004, *ApJ*, 601, 37
- Kazantzidis S., Zenter A., Kravtsov A., 2006, *ApJ*, 641, 647
- King I.R., 1966, *AJ*, 71, 65
- Mateo M.L., 1998, *ARA&A*, 36, 435
- McConnachie, A. W., Irwin, M. J., Ibata, R. A., Ferguson, A. M. N., Lewis, G. F., & Tanvir, N. 2003, *MNRAS*, 343, 1335
- McConnachie, A. W., Irwin, M. J., Lewis, G. F., Ibata, R. A., Chapman, S. C., Ferguson, A. M. N., & Tanvir, N. R. 2004, *MNRAS*, 351, L94
- McConnachie A. W., Irwin M.J., 2006, *MNRAS*, 365, 1263
- Miyamoto M., Nagai R., 1975, *Publ. Astron. Soc. Japan*, 27, 533
- Moore, B., Ghigna, S., Governato, F., Lake, G., Quinn, T., Stadel, J., & Tozzi, P. 1999, *ApJ*, 524, L19
- Navarro J., Frenk C.S., White S.D.M., 1997, *ApJ*, 490, 493
- Peñarrubia J.; Kroupa P. ; Boily C.M., 2002, *MNRAS*, 333, 779
- Peñarrubia, J. et al., 2005, *ApJ*, 626, 128
- Peñarrubia, J., Benson, A. J., Martínez-Delgado, D., & Rix, H. W. 2006, *ApJ*, 645, 240
- Quinn P.J, Goodman J., 1986, *ApJ*, 306, 472
- Toth, G., & Ostriker, J. P. 1992, *ApJ*, 389, 5
- Velazquez, H., & White, S. D. M. 1999, *MNRAS*, 304, 254
- Walker, I. R., Mihos, J. C., & Hernquist, L. 1996, *ApJ*, 460, 121
- Zucker, D. B., et al. 2004, *ApJ*, 612, L117